Title
Enhanced emission of fluorophores on shrink-induced wrinkled composite structures

Journal
Optical Materials Express, 4(4)

ISSN
2159-3930

Authors
Sharma, Himanshu
Digman, Michelle A
Felsinger, Natasha
et al.

Publication Date
2014-03-20

DOI
10.1364/OME.4.000753

Enhanced emission of fluorophores on shrink-induced wrinkled composite structures

Himanshu Sharma,[1] Michelle A. Digman,[2,4] Natasha Felsinger,[3] Enrico Gratton,[4] and Michelle Khine[1,3]

[1]*Deparment of Chemical Engineering & Materials Science, University of California, Irvine, California 92697, USA*
[2]*Department of Developmental and Cell Biology, Laboratory for Fluorescence Dynamics, University of California, Irvine, California 92697, USA*
[3]*Department of Biomedical Engineering, University of California, Irvine, California 92697, USA*
[4]*Department of Biomedical Engineering, Laboratory for Fluorescence Dynamics, University of California, Irvine, California 92697,USA*
**Email: mkhine@uci.edu*

Abstract: We introduce a manufacturable and scalable method for creating tunable wrinkled ferromagnetic-metallic structures to enhance fluorescence signals. Thin layers of nickel (Ni) and gold (Au) were deposited onto a pre-stressed thermoplastic (shrink wrap film) polymer. Heating briefly forced the metal films to buckle when the thermoplastic retracted, resulting in multi-scale composite 'wrinkles'. This is the first demonstration of leveraging the plasmons in such hybrid nanostructures by metal enhanced fluorescence (MEF) in the near-infrared wavelengths. We observed more than three orders of magnitude enhancement in the fluorescence signal of a single molecule of goat anti-mouse immunoglobulin G (IgG) antibody conjugated to fluorescein isothiocyanate, FITC, (FITC-IgG) by two-photon excitation with these structures. These large enhancements in the fluorescence signal at the nanoscale gaps between the composite wrinkles corresponded to shortened lifetimes due to localized surface plasmons. To characterize these structures, we combined fluctuation correlation spectroscopy (FCS), fluorescence lifetime imaging microscopy (FLIM), and two-photon microscopy to spatially and temporally map the hot spots with high resolution.

OCIS codes: (250.5403) Plasmonics; (180.4315) Nonlinear microscopy; (240.5770) Roughness; (240.0310) Thin films.

References and links

1. J. C. Waters, "Accuracy and precision in quantitative fluorescence microscopy," J. Cell Biol. **185**(7), 1135–1148 (2009).
2. A. Dorfman, N. Kumar, and J. I. Hahm, "Highly sensitive biomolecular fluorescence detection using nanoscale ZnO platforms," Langmuir **22**(11), 4890–4895 (2006).
3. G. L. Liu, J. Kim, Y. Lu, and L. P. Lee, "Fluorescence enhancement of quantum dots enclosed in Au nanopockets with subwavelength aperture," Appl. Phys. Lett. **89**(24), 241118 (2006).
4. A. Kinkhabwala, Z. F. Yu, S. H. Fan, Y. Avlasevich, K. Mullen, and W. E. Moerner, "Large single-molecule fluorescence enhancements produced by a bowtie nanoantenna," Nat. Photonics **3**(11), 654–657 (2009).
5. P. Zhu and H. G. Craighead, "Zero-mode waveguides for single-molecule analysis," Annu Rev Biophys **41**(1), 269–293 (2012).
6. R. M. Bakker, H. K. Yuan, Z. T. Liu, V. P. Drachev, A. V. Kildishev, V. M. Shalaev, R. H. Pedersen, S. Gresillon, and A. Boltasseva, "Enhanced localized fluorescence in plasmonic nanoantennae," Appl. Phys. Lett. **92**(4), 043101 (2008).
7. K. Balaa, E. Fort, and I. Nikon, "Surface plasmon enhanced TIRF imaging," Imaging & Microscopy **11**(4), 55–56 (2009).
8. Y. N. Xia and N. J. Halas, "Shape-controlled synthesis and surface plasmonic properties of metallic nanostructures," MRS Bull. **30**(05), 338–348 (2005).
9. Y. Fu, J. Zhang, and J. R. Lakowicz, "Plasmonic enhancement of single-molecule fluorescence near a silver nanoparticle," J. Fluoresc. **17**(6), 811–816 (2007).

#202274 - $15.00 USD Received 3 Dec 2013; revised 27 Jan 2014; accepted 28 Jan 2014; published 20 Mar 2014

10. L. C. Estrada, M. J. Roberti, S. Simoncelli, V. Levi, P. F. Aramendía, and O. E. Martínez, "Detection of low quantum yield fluorophores and improved imaging times using metallic nanoparticles," J. Phys. Chem. B **116**(7), 2306–2313 (2012).
11. W. L. Barnes, "Surface plasmon-polariton length scales: a route to sub-wavelength optics," J. Opt. A, Pure Appl. Opt. **8**(4), S87–S93 (2006).
12. W. L. Barnes, "Fluorescence near interfaces: the role of photonic mode density," J. Mod. Opt. **45**(4), 661–699 (1998).
13. L. Novotny, R. X. Bian, and X. S. Xie, "Theory of nanometric optical tweezers," Phys. Rev. Lett. **79**(4), 645–648 (1997).
14. K. Uetsuki, P. Verma, P. Nordlander, and S. Kawata, "Tunable plasmon resonances in a metallic nanotip-film system," Nanoscale **4**(19), 5931–5935 (2012).
15. N. C. Lindquist, T. W. Johnson, P. Nagpal, D. J. Norris, and S. H. Oh, "Plasmonic nanofocusing with a metallic pyramid and an integrated C-shaped aperture," Sci Rep **3**, 1857 (2013).
16. V. Ntziachristos, "Going deeper than microscopy: the optical imaging frontier in biology," Nat. Methods **7**(8), 603–614 (2010).
17. M. A. Albota, C. Xu, and W. W. Webb, "Two-photon fluorescence excitation cross sections of biomolecular probes from 690 to 960 nm," Appl. Opt. **37**(31), 7352–7356 (1998).
18. Y. Zhang, B. Kim, S. Yao, M. V. Bondar, and K. D. Belfield, "Controlled aggregation and enhanced two-photon absorption of a water-soluble squaraine dye with a poly(acrylic acid) template," Langmuir **29**(35), 11005–11012 (2013).
19. J. H. Vella and A. M. Urbas, "Nanoplasmonic array enhancement of two-photon absorption in a dye film," J. Phys. Chem. C **116**(32), 17169–17173 (2012).
20. W. Wenseleers, F. Stellacci, T. Meyer-Friedrichsen, T. Mangel, C. A. Bauer, S. J. K. Pond, S. R. Marder, and J. W. Perry, "Five orders-of-magnitude enhancement of two-photon absorption for dyes on silver nanoparticle fractal clusters," J. Phys. Chem. B **106**(27), 6853–6863 (2002).
21. H. Kano and S. Kawata, "Two-photon-excited fluorescence enhanced by a surface plasmon," Opt. Lett. **21**(22), 1848–1850 (1996).
22. I. Cohanoschi, S. Yao, K. D. Belfield, and F. E. Hernandez, "Effect of the concentration of organic dyes on their surface plasmon enhanced two-photon absorption cross section using activated Au nanoparticles," J. Appl. Phys. **101**(8), 086112 (2007).
23. J. Wenger, D. Gérard, H. Aouani, and H. Rigneault, "Disposable microscope objective lenses for fluorescence correlation spectroscopy using latex microspheres," Anal. Chem. **80**(17), 6800–6804 (2008).
24. D. Punj, M. Mivelle, S. B. Moparthi, T. S. van Zanten, H. Rigneault, N. F. van Hulst, M. F. García-Parajó, and J. Wenger, "A plasmonic 'antenna-in-box' platform for enhanced single-molecule analysis at micromolar concentrations," Nat. Nanotechnol. **8**(7), 512–516 (2013).
25. Y. Mély, G. Duportail, and L. A. Bagatolli, *Fluorescent Methods to Study Biological Membranes* (Springer, 2013)
26. K. M. Berland, P. T. So, Y. Chen, W. W. Mantulin, and E. Gratton, "Scanning two-photon fluctuation correlation spectroscopy: particle counting measurements for detection of molecular aggregation," Biophys. J. **71**(1), 410–420 (1996).
27. Y. X. Zhang, A. Dragan, and C. D. Geddes, "Broad wavelength range metal-enhanced fluorescence using nickel nanodeposits," J. Phys. Chem. C **113**(36), 15811–15816 (2009).
28. S. M. Williams, A. D. Stafford, K. R. Rodriguez, T. M. Rogers, and J. V. Coe, "Accessing surface plasmons with Ni microarrays for enhanced IR absorption by monolayers," J. Phys. Chem. B **107**(43), 11871–11879 (2003).
29. J. Chen, P. Albella, Z. Pirzadeh, P. Alonso-González, F. Huth, S. Bonetti, V. Bonanni, J. Akerman, J. Nogués, P. Vavassori, A. Dmitriev, J. Aizpurua, and R. Hillenbrand, "Plasmonic nickel nanoantennas," Small **7**(16), 2341–2347 (2011).
30. M. Pohl, L. E. Kreilkamp, V. I. Belotelov, I. A. Akimov, A. N. Kalish, N. E. Khokhlov, V. J. Yallapragada, A. V. Gopal, M. Nur-E-Alam, M. Vasiliev, D. R. Yakovlev, K. Alameh, A. K. Zvezdin, and M. Bayer, "Tuning of the transverse magneto-optical Kerr effect in magneto-plasmonic crystals," New J. Phys. **15**(7), 075024 (2013).
31. J. Lim and S. A. Majetich, "Composite magnetic-plasmonic nanoparticles for biomedicine: manipulation and imaging," Nano Today **8**(1), 98–113 (2013).
32. J. F. Torrado, J. B. González-Díaz, M. U. González, A. García-Martín, and G. Armelles, "Magneto-optical effects in interacting localized and propagating surface plasmon modes," Opt. Express **18**(15), 15635–15642 (2010).
33. A. R. Halpern and R. M. Corn, "Lithographically patterned electrodeposition of gold, silver, and nickel nanoring arrays with widely tunable near-infrared plasmonic resonances," ACS Nano **7**(2), 1755–1762 (2013).
34. V. I. Belotelov, I. A. Akimov, M. Pohl, V. A. Kotov, S. Kasture, A. S. Vengurlekar, A. V. Gopal, D. R. Yakovlev, A. K. Zvezdin, and M. Bayer, "Enhanced magneto-optical effects in magnetoplasmonic crystals," Nat. Nanotechnol. **6**(6), 370–376 (2011).
35. D. Regatos, B. Sepúlveda, D. Fariña, L. G. Carrascosa, and L. M. Lechuga, "Suitable combination of noble/ferromagnetic metal multilayers for enhanced magneto-plasmonic biosensing," Opt. Express **19**(9), 8336–8346 (2011).

#202274 - $15.00 USD Received 3 Dec 2013; revised 27 Jan 2014; accepted 28 Jan 2014; published 20 Mar 2014

36. G. Armelles, A. Cebollada, A. Garcia-Martin, and M. U. Gonzalez, "Magnetoplasmonics: combining magnetic and plasmonic functionalities," Adv. Opt. Mater. **1**(1), 10–35 (2013).
37. V. V. Temnov, G. Armelles, U. Woggon, D. Guzatov, A. Cebollada, A. Garcia-Martin, J. M. Garcia-Martin, T. Thomay, A. Leitenstorfer, and R. Bratschitsch, "Active magneto-plasmonics in hybrid metal-ferromagnet structures," Nat. Photonics **4**(2), 107–111 (2010).
38. J. Y. Chin, T. Steinle, T. Wehlus, D. Dregely, T. Weiss, V. I. Belotelov, B. Stritzker, and H. Giessen, "Nonreciprocal plasmonics enables giant enhancement of thin-film Faraday rotation," Nat Commun **4**, 1599 (2013).
39. J. C. Banthí, D. Meneses-Rodríguez, F. García, M. U. González, A. García-Martín, A. Cebollada, and G. Armelles, "High magneto-optical activity and low optical losses in metal-dielectric Au/Co/Au-SiO_2 magnetoplasmonic nanodisks," Adv. Mater. **24**(10), OP36–OP41 (2012).
40. S. Jayadev, J. Pegan, D. Dyer, J. McLane, J. Lim, and M. Khine, "Adaptive wettability-enhanced surfaces ordered on molded etched substrates using shrink film," Smart Mater. Struct. **22**(1), 014014 (2013).
41. L. R. Freschauf, J. McLane, H. Sharma, and M. Khine, "Shrink-induced superhydrophobic and antibacterial surfaces in consumer plastics," PLoS ONE **7**(8), e40987 (2012).
42. D. Nawarathna, N. Norouzi, J. McLane, H. Sharma, N. Sharac, T. Grant, A. Chen, S. Strayer, R. Ragan, and M. Khine, "Shrink-induced sorting using integrated nanoscale magnetic traps," Appl. Phys. Lett. **102**(6), 063504 (2013).
43. B. Zhang and T. Cui, "Tunable shrink induced graphene composites for chemical sensors and microfluidics," Proc. IEEE Micr. Elect. 1360–1363, (2012).
44. J. D. Pegan, A. Y. Ho, M. Bachman, and M. Khine, "Flexible shrink-induced high surface area electrodes for electrochemiluminescent sensing," Lab Chip **13**(21), 4205–4209 (2013).
45. C. C. Fu, A. Grimes, M. Long, C. G. L. Ferri, B. D. Rich, S. Ghosh, S. Ghosh, L. P. Lee, A. Gopinathan, and M. Khine, "Tunable nanowrinkles on shape memory polymer sheets," Adv. Mater. **21**(44), 4472–4476 (2009).
46. C. C. Fu, G. Ossato, M. Long, M. A. Digman, A. Gopinathan, L. P. Lee, E. Gratton, and M. Khine, "Bimetallic nanopetals for thousand-fold fluorescence enhancements," Appl. Phys. Lett. **97**(20), 203101 (2010).
47. M. D. Huntington, C. J. Engel, A. J. Hryn, and T. W. Odom, "Polymer nanowrinkles with continuously tunable wavelengths," ACS Appl. Mater. Interfaces **5**(13), 6438–6442 (2013).
48. C. M. Gabardo, Y. J. Zhu, L. Soleymani, and J. M. Moran-Mirabal, "Bench-top fabrication of hierarchically structured high-surface-area electrodes," Adv. Funct. Mater. **23**(24), 3030–3039 (2013).
49. C. G. L. Ferri, R. H. Inman, B. Rich, A. Gopinathan, M. Khine, and S. Ghosh, "Plasmon-induced enhancement of intra-ensemble FRET in quantum dots on wrinkled thin films," Opt. Mater. Express **3**(3), 383–389 (2013).
50. L. Zhang, X. Y. Lang, A. Hirata, and M. W. Chen, "Wrinkled nanoporous gold films with ultrahigh surface-enhanced Raman scattering enhancement," ACS Nano **5**(6), 4407–4413 (2011).
51. H. W. Liu, L. Zhang, X. Y. Lang, Y. Yamaguchi, H. S. Iwasaki, Y. S. Inouye, Q. K. Xue, and M. W. Chen, "Single molecule detection from a large-scale SERS-active $Au_{79}Ag_{21}$ substrate," Sci. Rep. **1**, 1–5 (2011).
52. A. Chen, E. Lee, R. Tu, K. Santiago, A. Grosberg, C. Fowlkes, and M. Khine, "Integrated platform for functional monitoring of biomimetic heart sheets derived from human pluripotent stem cells," Biomaterials **35**(2), 675–683 (2014).
53. A. Chen, D. K. Lieu, L. Freschauf, V. Lew, H. Sharma, J. X. Wang, D. Nguyen, I. Karakikes, R. J. Hajjar, A. Gopinathan, E. Botvinick, C. C. Fowlkes, R. A. Li, and M. Khine, "Shrink-film configurable multiscale wrinkles for functional alignment of human embryonic stem cells and their cardiac derivatives," Adv. Mater. **23**(48), 5785–5791 (2011).
54. Y. Y. Li, S. X. Dai, J. John, and K. R. Carter, "Superhydrophobic surfaces from hierarchically structured wrinkled polymers," ACS Appl. Mater. Interfaces **5**(21), 11066–11073 (2013).
55. V. A. Trofimov and E. B. Tereshin, "Localization of light energy of a femtosecond laser pulse upon generation of the second harmonic in a one-dimensional nonlinear photonic crystal with alternating nonlinear response," Opt. Spectrosc. **104**(5), 737–743 (2008).
56. P. T. C. So, C. Y. Dong, B. R. Masters, and K. M. Berland, "Two-photon excitation fluorescence microscopy," Annu. Rev. Biomed. Eng. **2**(1), 399–429 (2000).
57. M. Rubart, "Two-photon microscopy of cells and tissue," Circ. Res. **95**(12), 1154–1166 (2004).
58. K. T. Takasaki, J. B. Ding, and B. L. Sabatini, "Live-cell superresolution imaging by pulsed STED two-photon excitation microscopy," Biophys. J. **104**(4), 770–777 (2013).
59. J. L. Valverde, *Blood, Plasma, and Plasma Proteins: A Unique Contribution to Modern Healthcare* (IOS Press, 2006)
60. W. H. Zhang, F. Ding, W. D. Li, Y. X. Wang, J. Hu, and S. Y. Chou, "Giant and uniform fluorescence enhancement over large areas using plasmonic nanodots in 3D resonant cavity nanoantenna by nanoimprinting," Nanotechnology **23**(22), 225301 (2012).
61. T. Lohmüller, L. Iversen, M. Schmidt, C. Rhodes, H. L. Tu, W. C. Lin, and J. T. Groves, "Single molecule tracking on supported membranes with arrays of optical nanoantennas," Nano Lett. **12**(3), 1717–1721 (2012).
62. C. D. Geddes, A. Parfenov, D. Roll, I. Gryczynski, J. Malicka, and J. R. Lakowicz, "Silver fractal-like structures for metal-enhanced fluorescence: enhanced fluorescence intensities and increased probe photostabilities," J. Fluoresc. **13**(3), 267–276 (2003).
63. M. A. Digman, V. R. Caiolfa, M. Zamai, and E. Gratton, "The phasor approach to fluorescence lifetime imaging analysis," Biophys. J. **94**(2), L14–L16 (2008).

#202274 - $15.00 USD Received 3 Dec 2013; revised 27 Jan 2014; accepted 28 Jan 2014; published 20 Mar 2014

64. C. Stringari, A. Cinquin, O. Cinquin, M. A. Digman, P. J. Donovan, and E. Gratton, "Phasor approach to fluorescence lifetime microscopy distinguishes different metabolic states of germ cells in a live tissue," Proc. Natl. Acad. Sci. U.S.A. **108**(33), 13582–13587 (2011).
65. J. R. Lakowicz, J. Malicka, J. Huang, Z. Gryczynski, and I. Gryczynski, "Ultrabright fluorescein-labeled antibodies near silver metallic surfaces," Biopolymers **74**(6), 467–475 (2004).
66. C. Tregidgo, J. A. Levitt, and K. Suhling, "Effect of refractive index on the fluorescence lifetime of green fluorescent protein," J. Biomed. Opt. **13**(3), 031218 (2008).

1. Introduction

A persistent challenge in fluorescence microscopy is to increase the signal to noise ratio of weakly fluorescent biomarkers or of biomolecules present at low concentration [1, 2]. Strategies to increase both the quantum yield of the dye as well as to reduce the excitation volume have been demonstrated using nanoplasmonic structures such as gold (Au) bowtie antennas, zero-mode waveguides, nanoparticles, and thin films [3–7]. These strategies have significantly enhanced fluorescence signals due to near field plasmonic interactions. This enhancement known as metal enhanced fluorescence (MEF) is believed to be a combination of two mechanisms [8]. In the first, the interaction of the field from the incident light at a specific frequency with the free electrons on the metal surface induces a strong localized electromagnetic (EM) field concentrated at the vicinity of the metal nanostructures. In the second, the near-field interaction of the dipole moment of the fluorophore couples with the metal surface to generate spatial oscillations of the electron density referred to as localized surface plasmon resonance (LSPR). This LSP field can increase the excitation field and the radiative emission rate of the fluorophore. A fluorophore in the near-field (within tens of nanometers) can have a significantly enhanced radiative emission rate and shortened lifetime. A shortening in the inherent lifetime of the fluorophore increases its photostability [9]. However, if the fluorophore is in contact with the metallic surface, the molecular dipole of the fluorophore can directly and non-radiatively transfer its energy to the metal surface, such that the signal is quenched.

The optical properties and enhanced localized electromagnetic fields of these metallic nanostructures are strongly dependent on the composition, size, shape, and dielectric properties of the substrate and medium above the surface [10]. Early studies indicated that nanoscale confinement of the EM field within sub-wavelength volumes could enhance the field strength by several orders of magnitude relative to the incident light [11–13]. Furthermore, metallic nanostructures with sharp corners or tips could further enhance the local electric field [14, 15].

Two-photon excitation is leveraged extensively for biological imaging studies because in the near infrared region, there is less scattering loss, reduced photodamage, and a greater penetration depth [16]. Efforts to improve the performance of two-photon excitation fluorescence (TPEF) have been achieved mainly by using Au nanoplasmonic substrates to enhance the two-photon absorption (TPA) cross-sections of dyes [17–22]. These studies showed that aggregated metallic clusters had extremely strong localized electric field enhancement effects resulting in improving the TPA cross-sections of chromophores.

Fluctuation correlation spectroscopy (FCS) has also emerged as another powerful technique that has the ability to detect low concentrations of biomolecules [23, 24]. In this method, the spontaneous fluctuations in the fluorescence intensity can elucidate a wide variety of information about the molecule such as the local molecular concentrations, mobility coefficients, binding rates, and inter or intramolecular reactions [25]. However, the optimal biomolecule concentration has to be within the nM to 1 μM regime to observe few events [26]. Thus integrating the advantages of FCS with TPEF into a nanoplasmonic device could serve to be a useful method for detecting higher concentrations of weakly fluorescent biomarkers.

Recently studies have demonstrated that a ferromagnetic material such as nickel (Ni) has the optical properties to support plasmons in the near-infrared to infrared region [27, 28].

#202274 - $15.00 USD Received 3 Dec 2013; revised 27 Jan 2014; accepted 28 Jan 2014; published 20 Mar 2014

However, one of the main disadvantages with using pure ferromagnetic materials is the strong absorption losses that occur resulting in a strong damping of the surface plasmonic features [29, 30]. To overcome this damping, there has been significant interest in combining ferromagnetic materials with noble metals to create hybrid structures for increasing the plasmonic response [29, 31, 32]. These composite structures, also referred to as magnetoplasmonic structures, have demonstrated that magneto-optical effects such as the Faraday and Kerr effect fields can be implemented to control the surface plasmon propagation along nanostructured surfaces [29, 33–39]. We present here the first demonstration of leveraging the plasmons in Ni/Au composite structures for enhanced fluorescence signal by MEF in the near-infrared wavelengths.

We present a roll to roll compatible manufacturing process to create large areas of nanostructured bimetallic substrates fabricated by simply depositing Ni and Au thin films onto commodity shrink wrap polyolefin (PO) film. When the shrink film retracts, the thin stiffer metal films buckle to create 'wrinkle' structures [40–44]. This film shrinks considerably more than previously reported and thus results in significantly smaller structures [45–47]. A thin dielectric layer of silica (SiO_2) on top of the bimetallic structures serves as a spacer layer. We characterized our metallic structures by depositing goat anti-mouse immunoglobulin G (IgG) antibody conjugated to fluorescein isothiocyanate, FITC, (FITC-IgG) onto our composite structures and determined the enhancements in the fluorescence signal by a combination of two-photon microscopy, FCS, and fluorescence lifetime imaging microscopy (FLIM) to spatially and temporally map the hot spots on an MEF surface. Importantly, we were able to achieve significantly higher resolution than previously reported and show for the first time down to 33 nm resolution with FCS and correlate this with FLIM mapping [46]. FCS revealed that the hot spots observed are reduced to below the confocal volume, and FLIM shows a shorter lifetime present on the composite structures than in solution. This increase in the fluorescence signal and shortening in the fluorescence lifetime is due to the strong EM field localized around nanoscale gaps within our metallic structures. Finally, with this, we demonstrate we could detect single biomolecules by monitoring fluctuations in the fluorescence intensity of FITC-IgG antibody.

2. Fabrication and characterization of composite structures

Sharp tipped and closely packed metal structures have shown to be advantageous for fluorescence enhancement due to their ability to localize and concentrate the EM field around the surface of the metallic nanostructures when induced by illumination at a resonant frequency [46]. To create the composite structures, a similar fabrication approach is shown in Fig. 1(a). 1 mil thick pre-stressed PO shrink film (955-D, Sealed Air Corporation) laminated onto a 3 mil polyester backing was cleaned in isopropyl alcohol and dried with pressurized air. An array of holes, 2 mm in diameter, was created using CAD software (AUTOCAD, Autodesk, San Rafael, CA), and a carbon dioxide (CO_2) laser (VersaLaser VLS-2.30, Universal Laser Systems Inc. Scottsdale, AZ) was used to etch the array into sealing tape (Nunc sealing tape, Thermo Scientific, Rochester, NY). The laser cut tape acted as a mask for the deposition of metals onto the PO shrink film. The tape masks were then adhered on to the top of the PO pieces. For metal deposition, an ion beam sputter coater was used to accelerate 8 kV Ni, Au, and SiO_2 atoms from two ion guns (IBS/e South Bay Tech, San Clemente, CA) onto the masked PO pieces. The tape mask was removed from the metal coated PO pieces and substrates were shrunk by applying heat at 155 °C for 3 min. The PO shrink film contracts upon heating inducing the bimetallic film to buckle into sharp structures and create nano to submicron gaps between the wrinkle structures. This PO shrink film retracts by 95% in surface area, considerably more than previously reported [46]. As a result, smaller, sharper, and more densely packed wrinkled structures were thus created. Post-shrunk, 5 nm SiO_2 was ion-beam sputtered as the dielectric layer on top of the bimetallic structures to create the composite structures.

#202274 - $15.00 USD Received 3 Dec 2013; revised 27 Jan 2014; accepted 28 Jan 2014; published 20 Mar 2014

We deposited different thicknesses of Au on top of the PO shrink film and characterized the changes in surface topology using a scanning electron microscope (SEM) (FEI Magellan 400XHR SEM) and an atomic force microscope (AFM) (Asylum Research MFP-3D AFM). The Ni thickness was kept constant at 5 nm. Shrunk bimetallic substrates were sputter coated with 3 nm Au (Q150R S, Quorum Technologies) and SEM images were obtained with 5 kV beam and 4 mm working distance. Figures 1(b)-1(d) shows the SEM images of the composite structures and illustrates that by increasing the Au thickness from 10 nm to 30 nm, the wrinkles become less densely packed and the sharpness at the edges of the wrinkles dissipate, consistent with previous studies [45, 46]. The high magnification SEM images are used to show the various sizes of the gaps from nano to micron (20 nm to 6 μm) between the metal wrinkle structures within a representative 6 μm viewing window. Fast Fourier transform (FFT) analysis was used to estimate the sizes of the wrinkles. These SEM images reveal that the 10 nm Au structures had several nanogaps between the metallic structures followed by 20 nm Au and 30 nm Au. AFM height profiles reveal that similar to the heterogeneity in the structures observed from the SEM images, the heights of the composite structures varied up to greater than 3 μm.

These wrinkle structures are more controllable and robust than other heterogeneous structures, including the nanopetals which we have previously achieved large fluorescence enhancements [46]. Moreover, such wrinkle structures have been extensively characterized and leveraged for various applications [40–42, 44, 47–54]. Recent work has even shown that the wrinkles can be somewhat deterministic [47].

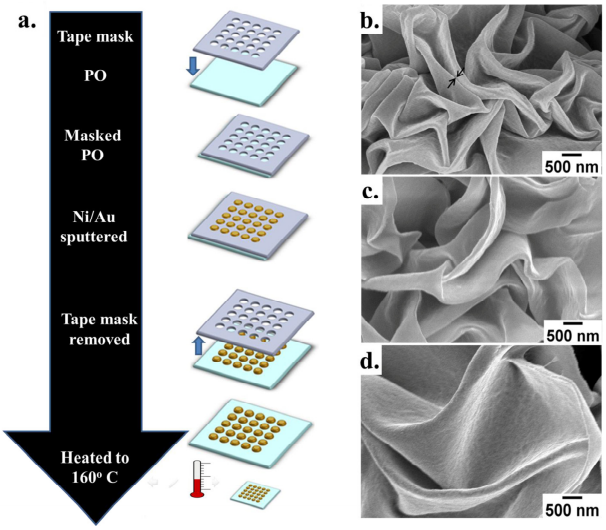

Fig. 1. Characterization of bimetallic structures (a) Process flow for creating islands of bimetallic structures on PO. SEM images of composite structures with different thickness of Au (b) 10 nm, (c) 20 nm, (d) 30 nm. Black arrow in (b) indicates a nanogap.

Recently, we demonstrated that with a very thin layer of Ni, effective ferro-magnetic nanotraps that localize strong magnetic fields can be formed with these wrinkles [42]. We found that increasing the Ni thickness to 30 nm increased the size and reduced the sharpness of the nanowrinkles and as a result decreased the magnetic strength. To determine the thickness for this study, Ni thickness was thus varied from 5 to 25 nm, leaving the Au thickness constant at 10 nm (Fig. 2). As expected and consistent with scaling laws, thicker layers of Ni resulted in larger structures presented in Figs. 2(a)-2(c). Therefore, for this study, 5 nm of Ni was used throughout.

#202274 - $15.00 USD Received 3 Dec 2013; revised 27 Jan 2014; accepted 28 Jan 2014; published 20 Mar 2014

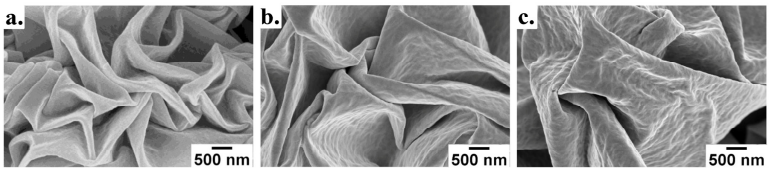

Fig. 2. SEM characterization of composite structures with fixed 10 nm Au and varying thicknesses of Ni (a) 5 nm, (b) 15 nm, (c) 25 nm.

3. Two-photon excitation of FITC-IgG on composite structures

Recent studies have shown that illuminating nanoscale metallic structures by a broadband femtosecond pulsed laser such as those used in two-photon microscopy can be an effective way to study the localization of light [46, 55]. One of the key advantages with using two-photon microscopy is that with this method, the fluorophore excitation is localized to the excitation focal volume which is generally within the femtoliter regime [56–58]. This is especially useful when studying fluorescence hotspots generated within nanoscale gaps. Furthermore, due to the nonlinear quadratic dependence of the two-photon excitation process, the intensity scales to the fourth power of the EM field in the metal.

1 μM FITC-IgG (Sigma-Aldrich, USA) prepared in phosphate buffered saline (PBS) was pipetted on top of the composite structures and sandwiched by a thin glass coverslip before being mounted on the Zeiss LSM 710 microscope. The microscope was coupled to a mode-locked two-photon titanium (Ti)-sapphire laser (Spectra-Physics, Mountain View, CA) operated at 785 nm with a 80-MHz repetition rate. Samples were imaged with a 40 × /1.2NA water immersion objective lens (C-Apochromat Water Corr, Carl Zeiss, Jena, Germany) and excited at 785 nm with a laser power of 150 μW. The emitted fluorescence light was selected by a spectral detector from 495 to 650 nm and detected by a photomultiplier tube. Images were captured at 8.5 μm X 8.5 μm zoom.

IgG was chosen as the model protein because it is one of the most abundant classes of immunoglobulin in blood [59]. FITC, a derivative of fluorescein, is one of the simplest and prevalently used fluorescent dyes for labeling peptides, proteins, and antibodies. Thus, for biological relevance, enhancing the fluorescence signal of FITC-IgG on the composite structures was chosen. As the fluorescently tagged antibodies diffused by Brownian motion, and passed within nanometer proximity over specific regions of the composite structures, the fluorescence signal was observed to suddenly burst, becoming significantly enhanced relative to the background signal. After the sudden burst in the fluorescence signal was observed, the signal immediately dropped, indicative of a hot spot [60, 61]. To determine the width of each of the bursts in the fluorescence signal, FCS line scanning was conducted.

FCS line scanning was obtained by scanning a line of length of 256 pixels 100,000 times, with a pixel size of 33 nm and a pixel dwell time of 1.00 μs to capture the rapidly diffusing molecules. An 8.5 μm horizontal line was scanned over the region where fluctuations in the intensity were observed. A time trace of the fluorescence intensity was collected for 60 seconds. Data analysis was processed by the SimFCS software developed at the Laboratory of Fluorescence Dynamics (LFD). Intensity data are presented using a carpet representation in which the *x*-coordinate corresponds to the point along the line (pixels) and the *y*-coordinate corresponds to the time of acquisition. Using the SimFCS program, the intensity data was thresholded from 2500 to 4095 which is the maximum measurable intensity to look at the counts with the higher intensities. The value of 2500 was selected as the minimum intensity threshold in order to only look at the intensities that were at least 10 fold higher than the background noise. The background noise was measured using the composite structures with PBS. The specific line with point(s) of intensity larger than 2500 counts was examined to determine the size of the hot spot and the duration of the intensity fluctuation.

#202274 - $15.00 USD Received 3 Dec 2013; revised 27 Jan 2014; accepted 28 Jan 2014; published 20 Mar 2014

Figure 3(a) presents the line scan carpet image for a region where a burst in the intensity signal was observed. The high fluorescence intensities are color coded red while the background and areas of lower fluorescence are color coded blue. Figure 3(b) illustrates that the sudden increases in the fluorescence intensity occur for only one pixel and are at most 1 μs before dropping to the less enhanced signal. An estimation of the enhancement in the fluorescence signal reveals that more than three orders of magnitude relative to glass was observed. The horizontal line profile also argues against the fact that the bright signals are due to aggregation effects; if such were the case, the intense fluorescence signal would last several pixels long. Furthermore, these findings are consistent with previous work that have shown that as the gaps between metallic structures become less than 50 nm, the fluorescence signal significantly increases [24]. Since the diffusion coefficient of FITC-IgG is around 40-50 $\mu m^2/s$, the molecules are moving relatively fast and the hotspots would only be observed for a brief time. Figure 3(b) reveals that these short bursts in the fluorescence signal were not observed on the control samples which were the composite structures with PBS, glass coverslip with PBS, and glass coverslip with FITC-IgG. This further supports that these bursts in intensity are related to the near-field effects from interaction of FITC-IgG with the composite structures and not due to possible artificial noise effects (i.e laser) or from the analog detector. The low level fluctuations in the signal observed on the control conditions, glass coverslip with PBS and FITC-IgG and composite structures with PBS were similar; we further confirmed that at 150 μW laser power, FITC-IgG on the glass coverslip was undetectable. While slight fluctuations in the signal occurred on the control samples, they were negligible relative to the magnitude increase in the fluorescence signal observed on the composite structures. Previously, amplitude analysis was used to estimate the hot spot volume because the spatial resolution was diffraction limited to ~300 nm [46]. In this work, using FCS to analyze the line scan data significantly improved the spatial resolution and quantified the hot spots to be less than 33 nm, translating to attoliter hotspot volumes. For the 1 μM FITC-IgG stock concentration pipetted on top of the composite structures, we can observe one molecule diffusing into the "hotspot" region at a time. To examine the number of times a single molecule diffuses to the "hotspot" region and becomes significantly brighter, a position in the sample was fixed and monitored for 60 seconds. Figure 3(c) illustrates that for a fixed position, multiple hotspots of comparable magnitudes occur. The vertical line profile also confirms that these short bursts in the fluorescence signal are not due to the FITC-IgG molecules adhering to the metallic surface; aggregation would result in the bright signal to last for several lines or more than the line time of 0.6 ms. The vertical line profile reveals that the enhancements in the signal achieved with these composite structures is comparable in intensity to those achieved with bimetallic nanopetals, but at a laser power that is almost 12 fold lower [46]. As expected, as the laser power was increased, an increase in the population of hot spots was noted. Since the intensity scales to the fourth power of the EM field in the metal in two-photon excitation, the enhancements achieved are significantly larger than previously demonstrated.

Figure 3(d) shows the histogram profile for the collection of line trace scans and illustrates that significantly brighter pixels are observed on the composite structures compared to the controls. The PBS on the composite structures has a slightly higher signal but does not produce a significant amount of background signal to contribute to the enhanced signals observed on the composite structures.

#202274 - $15.00 USD Received 3 Dec 2013; revised 27 Jan 2014; accepted 28 Jan 2014; published 20 Mar 2014

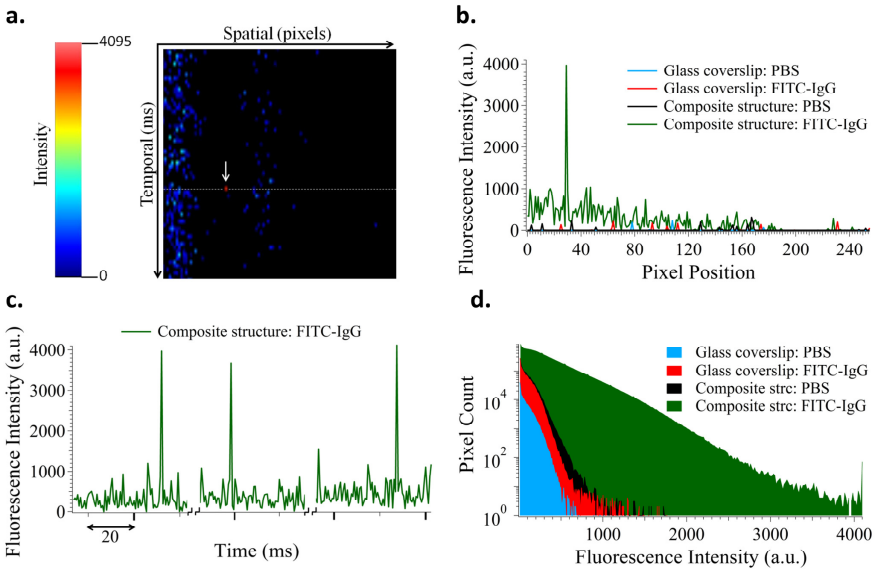

Fig. 3. Fluorescence line scan analysis of 1 µM FITC-IgG and PBS at 785 nm excitation on glass coverslip and composite structures (a) Fluorescence image from scanning FCS of composite structure where hotspots were observed indicated by white arrow (b) Horizontal line intensity profile for fixed time point (c) Vertical line intensity profile for a fixed pixel position collected for 60 sec (d) Histogram distribution profile of the fluorescence intensities.

If the increase in fluorescence signal is due to plasmonic effects, the lifetime of the fluorophore is also expected to be reduced [9, 62]. The phasor approach in the frequency domain has the ability to visualize and distinguish multiple species present in a mixture and can filter out unwanted artifacts such as erroneous background noise (i.e. room light) [63].

Fluorescence lifetime images were acquired with a Zeiss 710 microscope coupled to a Ti:Sapphire laser system. A 40X/1.2NA water immersion objective was used for imaging. For image acquisition the following settings were used: image size of 256 X 256 pixels and scan speed of 25 µm/pixel. A dichroic filter (760 nm) was used to separate the fluorescence signal from the laser light and the fluorescence emission was collected from 515 to 565 nm. For the acquisition of FLIM images, fluorescence was detected by a photomultiplier (H7422P-40, Hamamatsu, Japan) and a 610 nm short pass filter was placed in front of the detector. FLIM data was acquired and processed by the SimFCS software developed at the LFD. The excitation wavelength used was 785 nm. An average power of about 150µW was used to excite the FITC-IgG on the composite structures and 800 µW for FITC-IgG in solution. The FLIM calibration of the system was performed by measuring the known lifetime of fluorescein with a single exponential of 4.04 ns at a laser power of 800 µW. The phasor transformation and data analysis of the experiments was also performed using the SimFCS software, as described in previously published papers [64]. The phasor approach to FLIM converts at each pixel in an image the fluorescence decay histogram into the sine and cosine components. These components are then represented in a two dimensional histogram also referred to as a phasor plot. Each of the pixels in the image results in a single point in the phasor plot and when used in reciprocal mode, each point of the phasor plot can be mapped to each pixel in the image. The histogram was plotted by finding the average phasor, τ_p, in the program.

Figures 4(a)-4(c) display the FLIM images of FITC -IgG on the glass coverslip and on the composite structures as well as the phasor plot to map out where the fluorescence lifetimes lie for each pixel. Briefly, all points that are on the universal circle in the phasor plot have single exponential lifetimes which are related to one species while those inside the circle have

#202274 - $15.00 USD Received 3 Dec 2013; revised 27 Jan 2014; accepted 28 Jan 2014; published 20 Mar 2014

multiple exponential lifetimes. The fluorescence lifetime of FITC-IgG on glass is observed to be uniform and centered around 2.8 ns on the universal circle as depicted by the red color shown in Fig. 4(a) [65]. In contrast, on the composite structures with FITC-IgG, mapping the lifetimes from the FLIM image reveals a distribution of lifetime which extends from 2.8 ns to less than 50 ps. In our previous work, we performed FLIM by using the time correlated single photon counting card and were only able to present the average lifetime of the species in an image [46]. Here, using the phasor approach with FLIM, lifetime differences across the image can easily be observed and mapped. Mapping out where lifetimes shorter than 100 ps exist confirms that these lifetimes are observed in areas with high fluorescence intensity. This is also represented quantitatively by plotting out a normalized histogram of the lifetime values shown in Fig. 4(d). Similar to the FLIM map, the FITC-IgG on the glass coverslip is centered around 2.8 ns. In contrast, the histogram profile of the lifetime values for FITC-IgG on the composite structures has a range from 2.8 ns to mostly less than 50 ps, which is at the limit of the lifetime detection system. The observed decrease in lifetime on the composite structure at the points where the structures are the brightest is attributed to the enhancement of local excitation electric fields, leading to an increased excitation rate of fluorophores and radiative decay rate. This significant increase in the radiative decay rate implies an increase in the rate of emission of the fluorophore. The slight shifts in the fluorescence lifetime of FITC-IgG on the unenhanced regions on the composite structures could be due to changes in the refractive index which is known to also affect fluorescence lifetime [66].

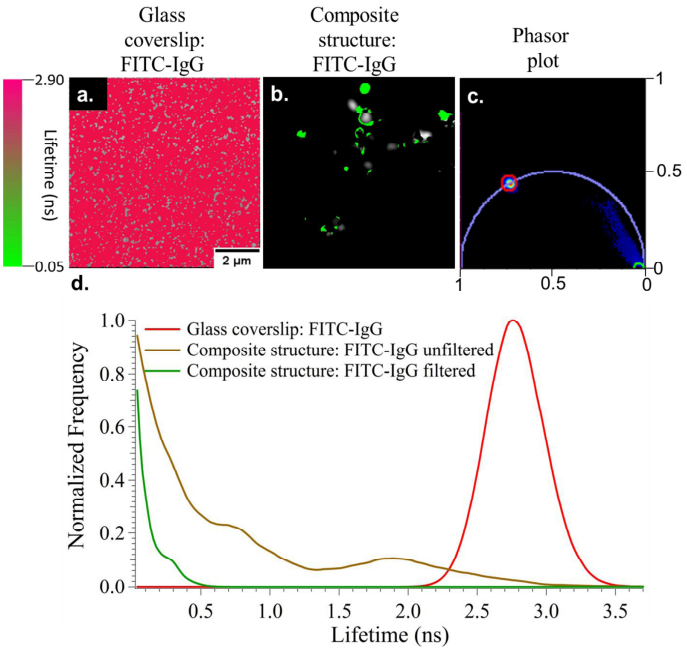

Fig. 4. Fluorescence lifetime analysis of 1 µM FITC-IgG at 785 nm excitation. (a) FLIM image on glass (b) FLIM image on composite structures (c) Phasor plot to show lifetime distribution (d) Normalized frequency profile of lifetimes.

4. Conclusion

The composite structures introduced here are able to enhance the fluorescence emission of labeled biomolecules by more than three orders of magnitude relative to a glass coverslip with two-photon excitation. The fluorescence enhancements observed occur by plasmonic effects due to the nanoscale gaps in the wrinkle structures. These structures can be tuned to have a diverse range of architectures and nanogap sizes with tunable plasmon resonances. This is

#202274 - $15.00 USD Received 3 Dec 2013; revised 27 Jan 2014; accepted 28 Jan 2014; published 20 Mar 2014

important to achieve large fluorescence enhancements in other regions of the excitation wavelength spectrum. We have also recently demonstrated that our Ni structures can generate strong localized magnetic gradients to serve as effective nanotraps for capture and separation [42]. Combining this utility with the large signal enhancements demonstrated here can pave the way to create a comprehensive integrated device to readily magnetically trap and sensitively detect labeled molecules and nanoparticles.

Acknowledgments

This work is supported by the National Institute of Health (NIH) through the DP2 NIH Director's New Innovator Award (1 DP2 OD007283-01) and M.A.D. and E.G. were supported in part by NIH grants P41-RRO3155, P41 GM103540, and P50-GM076516. SEM imaging was performed at the Laboratory for Electron and X-ray Instrumentation (LEXI) at UCI. The authors also thank Dr. Regina Ragan and Nick Sharac at UCI for help with AFM measurements.

#202274 - $15.00 USD Received 3 Dec 2013; revised 27 Jan 2014; accepted 28 Jan 2014; published 20 Mar 2014